applied sciences

MDPI

Article

Carbon Emission Calculation and Prediction of Asphalt Pavement Construction in Long Tunnel Based on Hybrid Life Cycle Assessment

Dan Yuan [1], Jian Wu [1,2], Qi Shi [2] and Dunwen Liu [1,*]

[1] School of Resources and Safety Engineering, Central South University, Changsha 410083, China; 255512045@csu.edu.cn (D.Y.)
[2] Road & Bridge South China Engineering Co., Ltd., Zhongshan 528403, China
* Correspondence: dunwen@csu.edu.cn

Abstract

Long asphalt tunnels serve as critical infrastructure for urban public transport, yet their construction entails substantial energy consumption and carbon emissions. This study aims to quantify and predict carbon emissions from asphalt pavement construction in long tunnels. Adopting Hybrid Life Cycle Assessment (HLCA), the asphalt paving process is divided into five stages: material production, transportation, on-site paving, milling, and ventilation. Four construction schemes are formulated via detailed calculation and analysis. A carbon emission factor database specific to long tunnel asphalt pavement construction in Guangxi is established, and a quantitative model is developed using the emission coefficient method to calculate carbon emissions of each scheme, among which Scheme 2 is determined as the optimal low-carbon construction scheme. The calculation model is validated via numerical software, and a carbon emission prediction dataset is constructed. Three prediction models, namely GA-BPNN, conventional SVR, and BPNN, are established. The results indicate that the GA-BPNN model achieves the highest predictive accuracy among the three models. This study further improves the calculation and prediction methods for carbon emissions in long tunnel asphalt pavement construction, providing theoretical support for carbon reduction and low-carbon construction management.

Keywords: long tunnel; carbon emission calculation; HLCA; carbon emission prediction; GA-BPNN

1. Introduction

In the 21st century, global warming has emerged as a major challenge to humanity [1]. The transportation sector is a major contributor to global carbon dioxide (CO_2) emissions [2]. To alleviate traffic congestion and optimize route alignments, long tunnels have become critical infrastructure in mountainous and urban highway networks. However, asphalt paving in long tunnels involves high energy consumption. Unlike open-road construction, the confined underground space requires continuous, high-power mechanical ventilation and specialized equipment operations to ensure worker safety and pavement quality [3,4]. Consequently, accurate quantification and prediction of carbon emissions present a key challenge for sustainable infrastructure development.

When accounting for carbon emissions in asphalt construction, conventional studies typically employ the Life Cycle Assessment (LCA) method for estimation. Liu Qi et al. [5]

Academic Editor: Luís Picado Santos

Received: 12 May 2026
Revised: 28 May 2026
Accepted: 28 May 2026
Published: 1 June 2026

utilized the LCA method to assess roadways, employing VISSIM and MOVES for calculating additional emissions resulting from congestion. Zhu Siyue et al. [6] applied the Process Life Cycle Assessment (PLCA), crafting an evaluation framework and computational model to gauge the energy and carbon footprints of three asphalt pavement maintenance materials—Thin Overlay (TO), Synchronous Surface Dressing (SSD), and Micro-surfacing (MS). Nonetheless, PLCA, as a down-top calculation approach, inevitably faces the challenge of "truncation error" during inventory data collection, where limitations in resources lead to an incomplete accounting boundary [7–9]. To address this limitation, some researchers have advocated for the top-down Input–Output Analysis (IOA) method [10–12]. However, this method can only furnish carbon emission accounting outcomes at a sectoral level. Given the constrained precision of sectoral segmentation, using sectoral emission levels to represent specific industries can introduce aggregation errors [8]. To leverage the strengths of both approaches, Suh et al. [7] and Heijungs et al. [13] merged PLCA and IOA to propose a Hybrid Life Cycle Assessment (HLCA) model. This methodology has found extensive application in life cycle energy consumption and carbon emission accounting for renewable energy [12,14–16]. Nevertheless, unlike on open roads, asphalt paving in long tunnels is constrained by the confined environment, so the application of carbon emissions assessments for asphalt paving in long tunnels requires further research.

In the realm of carbon emission prediction, researchers both domestically and internationally have conducted numerous studies. Chen et al. [17] developed various prediction models using machine learning algorithms for constructing a metro space and station in Chengdu city. They discovered that the Differential Evolution Levenberg–Marquardt (DELM) model exhibited superior prediction performance compared to other models. Zhao et al. [18] focused on carbon emissions in tunnel construction, initially employing random forest analysis to determine the importance ranking of parameter variables. They then integrated the Sparrow Search Algorithm (SSA), Gray Wolf Optimization Algorithm (GWO), and Genetic Algorithm (GA) with the Support Vector Regression (SVR) model. Their comparative analysis revealed that the SSA-SVR combination model achieved the highest predictive accuracy. Jassim [19] introduced an Artificial Neural Network (ANN) prediction model to assess the relationship between transported material volume units, energy consumption, and CO_2 emissions over varying transportation distances. The Back Propagation Neural Network (BPNN) within ANN is a widely utilized model with self-learning, adaptive, and non-linear mapping capabilities. However, determining thresholds and weights for BPNN involves some ambiguity and a lack of regularity, making it challenging to accurately and swiftly identify extreme values of non-linear functions [20,21]. Genetic Algorithm (GA) is a population optimization algorithm rooted in genetic evolution and natural selection principles, offering simple processing, high efficiency, and global optimization capabilities [22]. Consequently, this study employs a genetic algorithm (GA) to optimize a backpropagation neural network (BPNN) and construct a model for predicting carbon emissions during the construction of long tunnel asphalt pavements. This approach overcomes the limitations of traditional neural networks, such as the occurrence of local minima, and provides a more stable and accurate tool for emissions forecasting.

For this purpose, this study aims to develop a Hybrid Life Cycle Assessment (HLCA) model tailored for carbon emission assessment in low-carbon asphalt construction within long tunnels. A consistent accounting boundary will be employed to quantify and compare the carbon dioxide emissions associated with various construction alternatives. This study will analyze carbon emissions during the construction phase, their distribution, and the benefits of emission reductions, providing valuable data to support the sustainable development of asphalt construction in long tunnels in China. Additionally, a combination of the carbon emission factor method and computational software will be utilized to collect carbon emission data for diverse construction scenarios in the whole tunnel. Employing Matlab (2018b), the GA-BPNN prediction model will be developed and applied to forecast carbon emissions from asphalt construction in long tunnels, followed by an assessment of the model's predictive accuracy. Furthermore, traditional Support Vector Regression (SVR) and Back Propagation Neural Network (BPNN) carbon emission prediction models will be established, and their performance will be comprehensively evaluated using various assessment criteria.

2. Materials and Methods

The research methodology for investigating green construction practices and predicting carbon emissions from asphalt construction in long tunnels, based on the Hybrid Life Cycle Assessment (HLCA) framework established in this study, is illustrated in Figure 1. The key steps are outlined as follows:

(1) Initial Exploration Phase: Conduct a comprehensive literature review on tunnel asphalt construction, carbon emission accounting, and machine learning prediction methods; collect engineering design documents, construction logs, and equipment data; and perform theoretical analysis of HLCA principles and tunnel-specific carbon emission sources to define the research scope and system boundaries.

(2) Carbon Emission Accounting and Construction Scheme Comparison: Establish the construction phase HLCA model for tunnel asphalt pavement, including asphalt production, transportation, paving, milling, and ventilation. Calculate carbon emissions for different construction scenarios using emission factors, and compare results to identify low-carbon construction strategies.

(3) Dataset Preparation: Based on the accounting results, construct the prediction model dataset by extracting key input parameters (asphalt consumption, transportation distance, equipment power, ventilation duration, construction scale) and the corresponding output (total carbon emissions) from multiple construction scenarios. Preprocess the dataset in Matlab R2018b: normalize variables via min–max scaling, split into training (80%) and test (20%) sets, and remove outliers using the 3σ rule.

(4) Prediction Model Development and Evaluation: Using the preprocessed dataset, build three prediction models in Matlab: GA-BPNN (genetic algorithm-optimized back propagation neural network), SVR (support vector regression), and traditional BPNN. Evaluate model performance using metrics such as R^2, MSE, MAPE, TIC, and DA, and select the optimal model for carbon emission prediction.

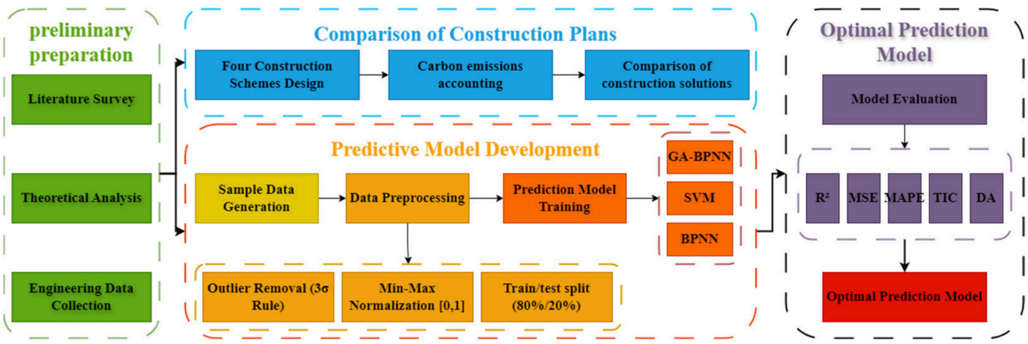

Figure 1. Flow chart of the study.

Subsequent sections will delve into three key aspects: an overview of the project, the HLCA methodology, and the GA-BPNN prediction model.

2.1. Project Overview

This study focuses on the reconstruction and expansion project of the Guangxi Guilin–Liuzhou section of the Quanzhou–Nanning Expressway. The route total length is 100.67 km, including a 35.2 km segment (Miaoling–Yongfu) with a design speed of 120 km/h and a 65.445 km segment (Yongfu–Luzhai North) with a design speed of 100 km/h.

As Figure 2 shows, the tunnel is a dual-bore, four-lane unidirectional highway tunnel located in Wujiatun, Guangfu Township, Yongfu County, Guilin. Its entrances and exits are located on the middle and lower parts of a hill, with only a small access road nearby. The left twin-bore tunnel ranges from Z-2K1177+335 to Z-2K1179+898 (2563 m), and the left single tunnel ranges from ZK1177+330 to ZK1179+895 (2565 m). The tunnel has small clearance openings and end-wall doors at both ends.

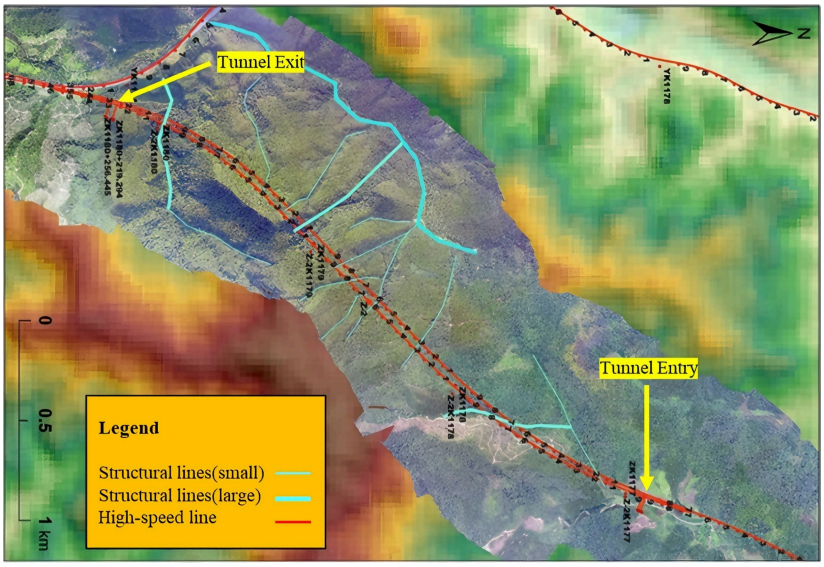

Figure 2. Tunnel structure diagram.

The tunnel adopts an asphalt concrete composite pavement structure (Figure 3): surface layer is 4 cm Stone Mastic Asphalt (SMA-13); lower asphalt layer is 8 cm medium-graded modified asphalt concrete (AC-20C); underlying layer is 28 cm C40 cement concrete slab; base layer is 18 cm C20 cement concrete; upper interlayer is water-stable permeable asphalt layer (emulsified PC-2), followed by two sealing layers (emulsified PC-1); asphalt binder layer (emulsified PC-3) is applied between asphalt layers; and the sealing layer (thickness $\geq$ 1 cm) is not included in the total structural thickness calculation.

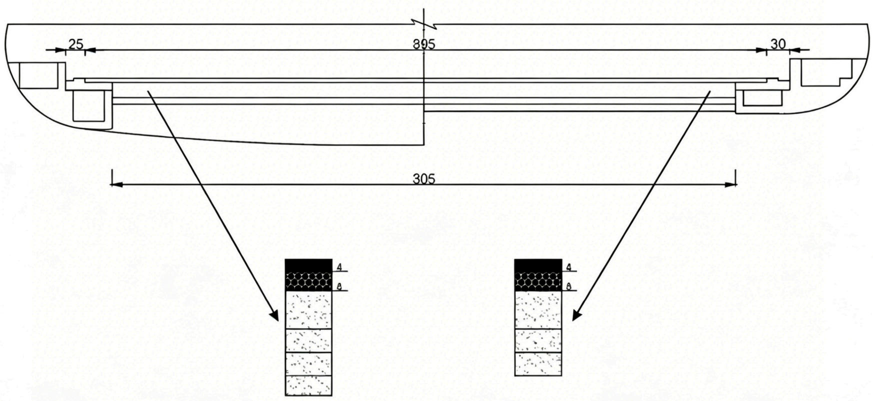

Figure 3. Tunnel asphalt concrete composite pavement.

2.2. Hybrid Life Cycle Assessment (HLCA)

2.2.1. System Boundaries and Functional Units

This study delves into the assessment of carbon emissions from asphalt pavement construction in long tunnels. Tunnel pavement construction was carried out from 30 July 2022 to 4 August 2022, with a total duration of 5 days. Owing to the long, confined underground space, continuous high-power ventilation is required, leading to higher energy consumption than conventional road construction. As illustrated in Figure 4, the system boundary is divided into three phases in line with the research scope: asphalt production, asphalt transportation, and on-site construction. The on-site construction stage includes asphalt paving, milling, and tunnel ventilation [23–27]. Additionally, due to the study's focus on the construction phase and data availability, machinery manufacturing, tunnel operation, routine maintenance, and final demolition disposal are not incorporated into the research boundary. To ensure consistency and comparability among different construction schemes, the functional unit of this study is uniformly defined as the total construction phase carbon emissions of the entire long tunnel asphalt pavement project. All calculations, comparisons, and analyses of carbon emissions in this study are based on the whole tunnel project. Furthermore, based on the following equations, we can obtain the construction phase carbon emissions per square meter (m^2) of asphalt pavement (unit: kg CO_2-eq/m^2), to facilitate horizontal comparison with other road and tunnel projects in published literature.

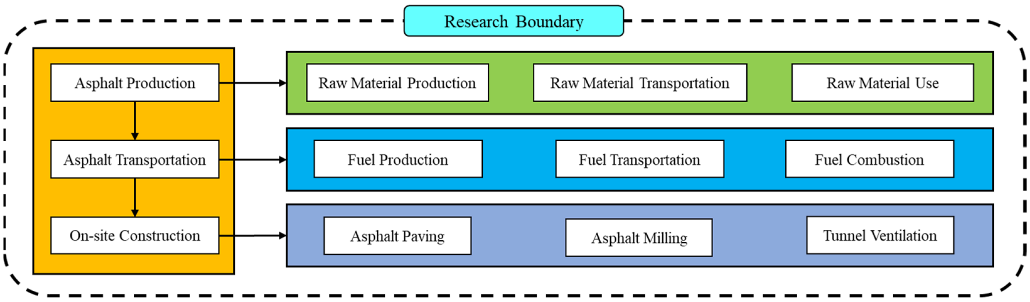

Figure 4. System boundary for construction-phase carbon emission assessment of tunnel asphalt pavement.

Based on the CO_2 emission sources illustrated in Figure 4, the CO_2 emission calculation formulas for each segment are presented as follows:

(1) CO_2 Emissions from the Construction and Operation of Asphalt Mixing Plants:

$$\begin{cases} P_1 = E_1 \times C_1 \\ P_2 = n_1 \times E_2 \times M_1 \end{cases} \tag{1}$$

where P_1 represents the CO_2 emissions from the construction of the asphalt mixing plant; E_1 denotes the carbon emission factor for the construction phase (derived from the construction sector IO emission factor (0.81 kg CO_2-eq/yuan, in Appendix A) from Chinese national input–output analysis.); C_1 indicates the total funds required for construction; P_2 represents the CO_2 emissions resulting from the operation of the asphalt mixing plant; n_1 signifies the number of asphalt mixing plants in operation; E_2 is the carbon emission factor associated with asphalt mixing plants of varying productivity (calibrated by fuel consumption + IO indirect emissions of mixing plant equipment.); and M_1 indicates the total number of operating shifts for the asphalt mixing plants.

(2) CO_2 Emissions from Labor Consumption:

$$P_3 = E_3 \times n_2 \times W \times d \tag{2}$$

where P_3 indicates the CO_2 emissions attributed to labor; E_3 is the carbon emission factor associated with labor consumption (includes both direct metabolism and indirect consumption from the residential sector IO table.); n_2 represents the number of laborers required for asphalt mixing plant operations; W signifies the average wage paid to laborers; and d denotes the number of working days.

(3) CO_2 Emissions from Asphalt Transportation:

$$P_4 = \frac{A \times \left(O_1 + \frac{X-1}{0.5} \times O_2\right)}{1000\rho} \tag{3}$$

where P_4 represents the CO_2 emissions associated with asphalt transportation; A denotes the total mass of asphalt being transported; O_1 indicates the carbon emissions produced during the first kilometer of transporting 1000 m^3 of asphalt (from JTG/T 3832-2018 [28]); X signifies the total distance of transportation; O_2 represents the carbon emissions for each additional 0.5 km of 1000 m^3 asphalt transportation; and ρ indicates the density of asphalt.

(4) CO_2 Emissions from the Asphalt Paving Process:

$$P_5 = \frac{A \times O_3}{1000\rho} \tag{4}$$

where P_5 represents the CO_2 emissions resulting from the paving process; O_3 indicates the carbon emissions produced by the paving of 1000 m^3 of asphalt.

(5) CO_2 Emissions from the Asphalt Milling Process:

$$P_6 = \frac{A \times O_4}{1000\rho} \tag{5}$$

where P_6 signifies the CO_2 emissions originating from the milling process; O_4 denotes the carbon emissions produced during the milling of 1000 m^3 of asphalt. Similar to the paving process, these coefficients are rigorously extracted from the national standard mechanical shift quotas.

(6) CO_2 Emissions from the Ventilation Process:

$$P_7 = E_4 \times n_3 \times d \times h \tag{6}$$

where P_7 indicates the CO_2 emissions generated by the ventilation process; E_4 represents the CO_2 emission coefficient for each 110 kW press-in ventilator. This coefficient is calculated by multiplying the ventilator's power (110 kW) by the latest Southern China Regional Power Grid Baseline Emission Factor; n_3 signifies the number of press-in ventilators used; d denotes the number of working days; h indicates the total number of working hours per day.

2.2.2. Construction of an HLCA Model

In accordance with the delineated system boundary, the primary factors influencing CO_2 emissions across each construction phase of asphalt construction in extended tunnels encompass the subsequent categories: (1) asphalt production; (2) electricity consumption during asphalt production; (3) fossil fuel consumption during asphalt production; (4) energy consumption during asphalt mixing plant construction and operation; (5) consumption related to construction machinery and equipment; (6) labor utilization. Illustrated in Figure 5, this study employs the hierarchical HLCA model [29–33] to quantify the CO_2 emissions associated with environmentally friendly asphalt construction in long tunnels.

Notably, the energy consumption during asphalt mixing plant construction and operation, as well as labor utilization, are deemed unsuitable for calculation via the LCA model. Moreover, the complexity of assessing construction equipment consumption via the LCA model necessitates an alternative approach. Consequently, the PLCA model is utilized to evaluate CO_2 emissions stemming from asphalt production, while the IOA model is applied to gauge CO_2 emissions arising from construction and operation energy consumption of asphalt mixing plants, construction equipment usage, and labor utilization.

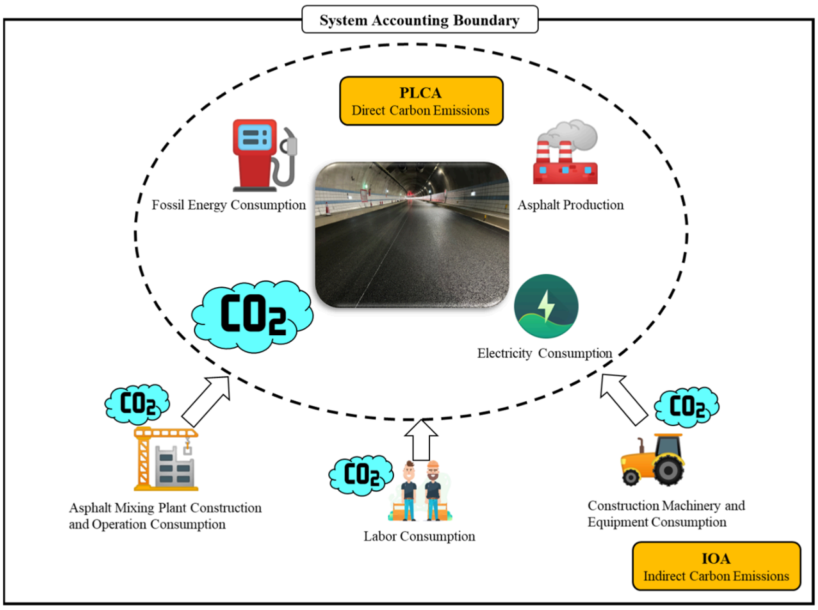

Figure 5. Illustration of carbon accounting for asphalt construction in long tunnels.

This study adopts a hybrid LCA (HLCA) framework by integrating Process LCA (PLCA) and Input–Output Analysis (IOA) to eliminate truncation errors and ensure system completeness. The core logic is that PLCA quantifies direct material and energy flows; IOA compensates for upstream indirect emissions; anti-double-counting rules are applied to avoid overlap. Among the PLCA parts applied to asphalt production are aggregate mining, bitumen refining, heating, mixing, and on-site paving, milling, and ventilation. All material inputs, fuel consumption, electricity, and mechanical operations are quantified using physical inventory data based on construction records and national standards (JTG/T 3832-2018). The IOA part is applied to four categories that cannot be fully decomposed into physical processes: Asphalt mixing plant construction and operation; construction machinery and equipment manufacturing and depreciation; labor-related indirect emissions; and external infrastructure and service consumption. The IOA module adopts the Chinese national input–output table and sectoral carbon emission inventory compiled by the National Bureau of Statistics; monetary values are converted to carbon emissions using sectoral average emission factors (kg CO_2-eq/yuan). The factors are derived from official energy statistics and carbon accounting guidelines (Guangxi and Southern China grid in Appendix A).

2.3. GA-BPNN

2.3.1. Principle of GA-BPNN

There are primarily three genetic algorithm optimization approaches for enhancing the performance of the BPNN. This research leverages genetic algorithms to optimize the initial weights and thresholds before the operation of the BPNN, with the aim of constructing a robust carbon emission prediction model. Specifically, before the BPNN operation, multiple sets of weights and thresholds are randomly generated. Subsequently, an appropriate encoding method is selected to encode each set of weights and thresholds, forming an individual, where each individual represents a solution set for BPNN. The genetic algorithm then proceeds to select, crossbreed, and mutate these individuals to identify the most optimal candidates from the pool. These optimal individuals are decoded and provided to the BPNN for training, facilitating the attainment of prediction results that converge towards the global optimum [34,35]. The process of GA-BPNN is depicted in Figure 6.

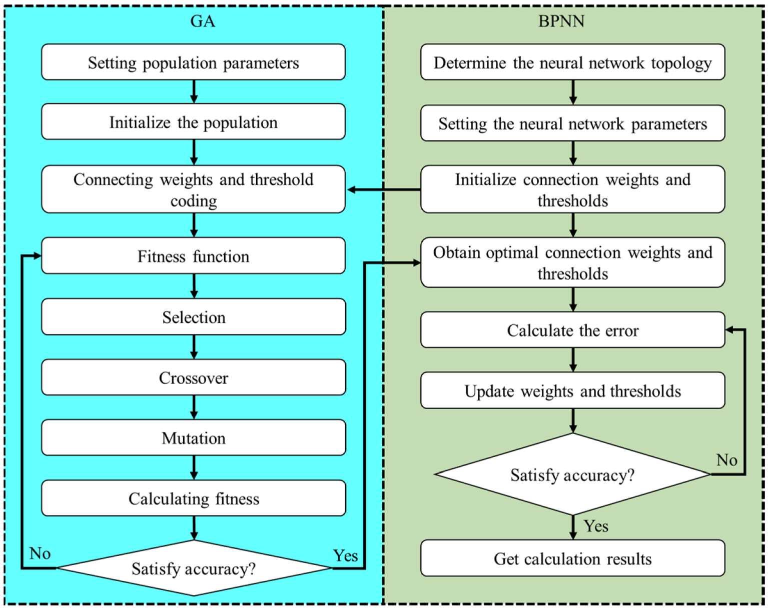

Figure 6. Flowchart of GA-BPNN.

2.3.2. GA-BPNN Model

(1) Determination and normalization of neural network topology

Within this investigation, input parameters including asphalt mixture output, diesel consumption, electricity consumption, gasoline consumption, and construction water consumption in the asphalt paving process of elongated tunnels are selected, with CO_2 emissions serving as the output parameter. A predictive model featuring a 5-N-1 topology is formulated, as depicted in Figure 7. The number of nodes, denoted as N, in the hidden layer significantly impacts the predictive accuracy of the network. An excessive number of nodes may lead to overfitting, while an insufficient number could elevate errors. Typically, the optimal range for N is determined by initially applying Equation (7) and subsequently employing a trial-and-error approach to ascertain the ideal quantity.

$$l = \sqrt{m+n} + \alpha \tag{7}$$

where m and n are the number of nodes in the input and output layers; α is a constant between 1 and 10.

Before the training of the neural network, to avoid the existence of order of magnitude differences between the input parameters affecting the predictive accuracy of the model, it is necessary to normalize them, and the calculation is shown in Equation (8):

$$x_i' = \frac{x_i - x_{min}}{x_{max} - x_{min}} \tag{8}$$

where x_i is the pre-normalized data; x_i' is the post-normalized data; x_{max} is the maximum value of the sample data; and x_{min} is the minimum value of the sample data.

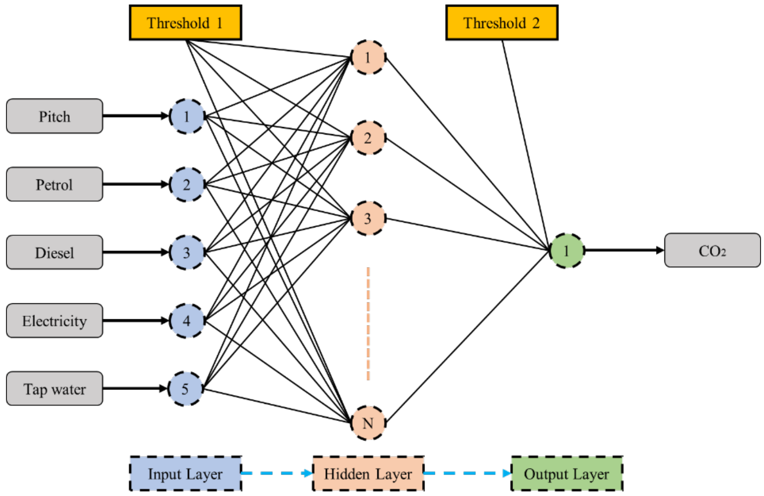

Figure 7. GA-BPNN topology (5 input–N hidden–1 output).

(2) Genetic algorithm coding

Genetic algorithms usually contain individuals with specific gene coding strings as processing objects, so the initial weights and thresholds need to be composed into individuals with reasonable encoding methods before model training. The encoding method is shown in Equation (9):

$$D = x \times y + y + y \times z + z \tag{9}$$

where $x \times y$ denotes the number of weights between the input layer and the hidden layer; y denotes the number of implicit layer thresholds; $y \times z$ denotes the number of weights between the implicit layer and the output layer; z denotes the number of output layer thresholds.

(3) Determination of the fitness function

In the BPNN, the root Mean Square Error (MSE) is the network operation of the accuracy of the requirements of the basis. When the root mean square error is smaller, it indicates that the accuracy of the fit is higher, at the same time indicating that at this time the weights and thresholds composed of the individual's adaptability are higher, and demonstrating the practicality of the calculation method, as shown in Equations (10) and (11):

$$E = \sqrt{\frac{1}{N}\sum_{i=1}^{N}(y_i - y_i')^2} \tag{10}$$

$$F = \frac{1}{E} \tag{11}$$

where E denotes the root mean square error; F is the fitness value; N is the number of testing samples; y_i is the actual value of the testing machine sample; y_i' is the predicted value of the testing set samples.

(4) Selection of genetic operators

Genetic operators in genetic algorithms mainly include selection operations, crossover operations, and mutation operations. The selection operation selects the fitness proportion method, whose basic idea is that the probability of an individual being selected and inherited to the next generation is directly proportional to its fitness value, and individuals with lower fitness also have a certain probability of being inherited to the next generation. The selection operation is shown in Equation (12):

$$p(x_i) = \frac{f(x_i)}{\sum_{j=1}^{N} f(x_i)} \tag{12}$$

where $p(x_i)$ is the probability that the ith individual is selected; $f(x_i)$ is the fitness value of the ith individual.

The crossover operation is selected as an arithmetic crossover, where two chromosomes are randomly selected from the population, and then the crossover points are randomly selected for crossover according to a certain crossover probability based on Equation (13).

$$\begin{cases} x'_k = x_k(1-b) + y_k b \\ y'_k = y_k(1-b) + x_k b \end{cases} \tag{13}$$

where x'_k and y'_k are the new individuals after crossover; x_k and y_k are the individuals before mutation; $b \in [1, 10]$. The mutation operation was chosen to be a non-uniform mutation, i.e., the probability of mutation occurring in different numbers of iterations was randomized, an individual was randomly selected from the population, and then one or more genes were randomly selected for mutation in the individual by the formula shown in Equations (14) and (15).

$$x'_k = \begin{cases} x_k + (x_{k,max} - x_k) \times f(g) \times \gamma_1 > 0.5 \\ x_k + (x_k - x_{k,min}) \times f(g) \times \gamma_1 \le 0.5 \end{cases} \tag{14}$$

$$f(g) = \gamma_2 (1 - \frac{g}{g_{max}})^2 \tag{15}$$

where $x_{k,max}$ is the maximum value of x_k; $x_{k,min}$ is the minimum value of x_k; and g is the current number of evolutionary generations of the individual.

3. Results and Analysis

3.1. Research on Green Construction of Asphalt in Long Tunnels Based on HLCA

3.1.1. Green Construction Option Design

The sequence of the asphalt construction process in long tunnels is production, transportation, paving, milling, and ventilation. According to asphalt pavement construction, first determine the production capacity of the selected asphalt mixing plant, and then select the various construction machinery to match it according to the regulations. The formula for calculating the production rate of the asphalt mixing plant [36,37] is as follows:

$$Q = \frac{L \times W \times H \times \rho}{M \times T \times K} \tag{16}$$

where Q stands for the mixing plant equipment asphalt mixture production efficiency (t/h); L stands for the paving length (m); W stands for the paving width (m); H stands for the paving thickness (m); ρ stands for the asphalt mixture compaction density (generally 2.2 t/m^3); M stands for the planned construction period (d); T stands for the daily running time (generally 16 h); K stands for the construction day factor (generally 0.8).

The total length of this tunnel is 5128 m, the thickness of the asphalt surface paving is 0.12 m, the average pavement width is 10 m, and the planned construction period is 5 d. The production capacity of the asphalt mixing plant in this tunnel can be calculated from Equation (16) to be more than 221 t/h. Combined with the research results [38,39] and

Appendix B, it is concluded that the asphalt production link-type pavement construction stage is the most important source of carbon emissions. Therefore, based on the combination of different asphalt mixing stations, the design of an asphalt green construction option for long tunnels is carried out.

The production scale of the asphalt mixing plant is divided into 30 t/h, 60 t/h, 120 t/h, and 240 t/h. Combined with the production requirements of the project, it is stipulated that each option shall not exceed five sets of production equipment, and four asphalt mixing plant construction options are designed to analyze the carbon emissions, and the transportation distance of the mixture is considered according to 3 km. Option 1: construction of one asphalt mixing plant with a production capacity of 240 t/h; Option 2: construction of two asphalt mixing plants with a production capacity of 120 t/h; Option 3: construction of one asphalt mixing plant with a production capacity of 120 t/h and two asphalt mixing plants with a production capacity of 60 t/h; Option 4: construction of one asphalt mixing plant with a production capacity of 120 t/h and four asphalt mixing plants with a production capacity of 30 t/h. The total production capacity of all four options is 240 t/h(the calculation criteria in Appendix B).

3.1.2. Comparison of Construction Options

The sources of CO_2 emissions from asphalt construction in this tunnel include production, transportation, paving, milling, and ventilation, as shown in Figure 8. Factors determining CO_2 emissions from production include the following: asphalt production, electricity consumption, fossil energy consumption, and asphalt mixing plant construction and operation consumption; factors determining CO_2 emissions from transportation include the following: construction machinery and equipment consumption, fossil energy consumption, and labor consumption; factors determining CO_2 emissions from paving include the following: construction machinery and equipment consumption, fossil energy consumption, and labor consumption; factors determining CO_2 emissions from milling include the following: construction machinery and equipment consumption, fossil energy consumption, and labor consumption; factors determining CO_2 emissions in the paving process include the following: consumption of construction machinery and equipment, fossil energy consumption, and labor consumption; and the factors determining CO_2 emissions in the ventilating process include the following: consumption of construction machinery and equipment, electrical energy consumption, and labor consumption.

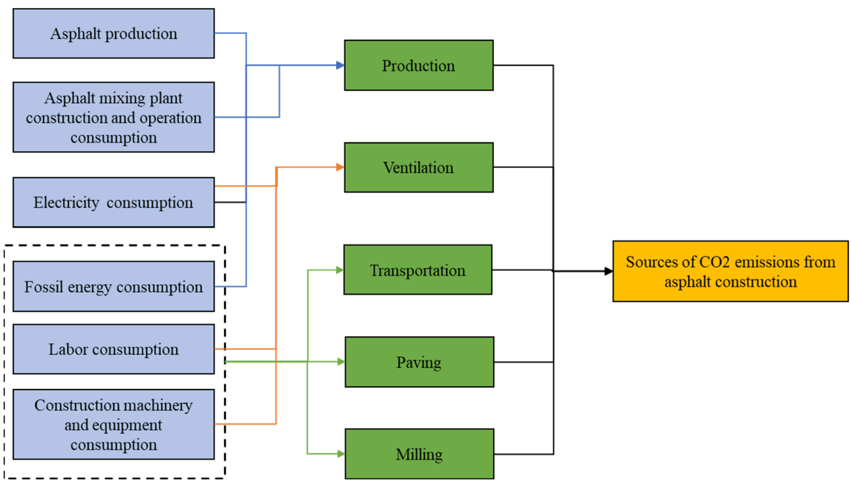

Figure 8. Sources of CO_2 emissions from asphalt construction.

The left and right sections of this tunnel are paved with asphalt. According to statistics, this tunnel uses a total of 6734.82 t of mix in the upper layer, 12,718.62 t of mix in the lower layer, and 213.61 t of mix in the permeable layer, adhesive layer, and sealing layer, totaling 19,667.05 t. The consumed quantities of asphalt construction machinery and labor accompanying each option are shown in Appendix C.

Based on the HLCA model established in Section 2.2, the total CO_2 emissions for the four proposed asphalt construction options were calculated. To maintain the readability of the main text, the highly detailed, step-by-step numerical substitutions and intermediate calculation processes for all options have been compiled in Appendix D.

A summary of the final calculated CO_2 emissions under different phases (mixing plant, labor, transportation, paving, and ventilation) is consolidated in Table 1.

Table 1. Carbon emissions of different construction schemes for the entire tunnel.

Section (kg)	Production Process	Transportation Process	Paving Process	Milling Process	Ventilation Process	Total
Option 1	20,690,601.53	19,533.47	8646.40	6226.92	4640.00	20,729,648.27
Option 2	18,259,099.12	19,533.47	8646.40	6226.92	4640.00	18,298,145.91
Option 3	19,206,461.78	19,533.47	8646.40	6226.92	4640.00	19,245,508.57
Option 4	19,204,774.84	19,533.47	8646.40	6226.92	4640.00	19,243,821.63

Upon scrutinizing Table 1 and juxtaposing the carbon emissions data associated with asphalt pavement construction in extended tunnels across various alternatives, it is evident that Option 2 exhibits the least total carbon emissions for the entire tunnel among the asphalt pavement construction choices. Option 2 demonstrates reductions in carbon emissions of 2,431,502.36 kg, 947,362.66 kg, and 945,675.72 kg when compared to Options 1, 3, and 4, respectively. Option 2 emerges as the optimal choice, showcasing superior performance in terms of carbon emissions, input cost, and construction schedule. Additionally, analysis of the percentage distribution of carbon emissions across the processes in the four scenarios reveals that the production process accounts for the highest percentage, while the ventilation process contributes the least. Consequently, optimizing the production process emerges as a pivotal area for further reducing carbon emissions.

To substantiate the aforementioned calculation methodology, the computational software was employed to compute the carbon emissions associated with the entire tunnel construction process. Given the intricate nature of calculating CO_2 emissions stemming from labor and asphalt mixing plant construction and operation through this software, validation was focused on verifying CO_2 emissions excluding these components. The software input data is delineated in Figure 9, yielding a resultant of 8,387,000 kg CO_2. A comparison with the CO_2 emission value derived from the earlier calculation of 8,379,100.38 kg reveals a close alignment, indicating a high level of accuracy in the calculation process.

Calculation outcomes from manual formula calculation and numerical software simulation are cross-checked. The two sets of data present consistent numerical values and changing tendencies.

According to widely adopted accuracy standards for road and tunnel construction carbon emission accounting, a relative error within ±5% is recognized as a reasonable and acceptable threshold for validating computational models. The deviation acquired in this comparison satisfies the above error criterion, which proves that the established accounting model has reliable calculation validity. The subtle numerical discrepancy mainly stems from two aspects: proper simplification of boundary conditions and parameter setting in software modelling, as well as numerical rounding generated in manual statistical computation. In terms of model sensitivity, parameters exert differentiated influences on final carbon emission values. Material consumption amount, mechanical operating hours, and regional basic emission factors belong to high-sensitivity variables, whose slight fluctuation can cause obvious changes in total emissions. By contrast, minor adjustments of auxiliary construction parameters exert negligible influence on the total emissions during the use phase. It indicates that the proposed model maintains stable operational performance under conventional construction condition variation.

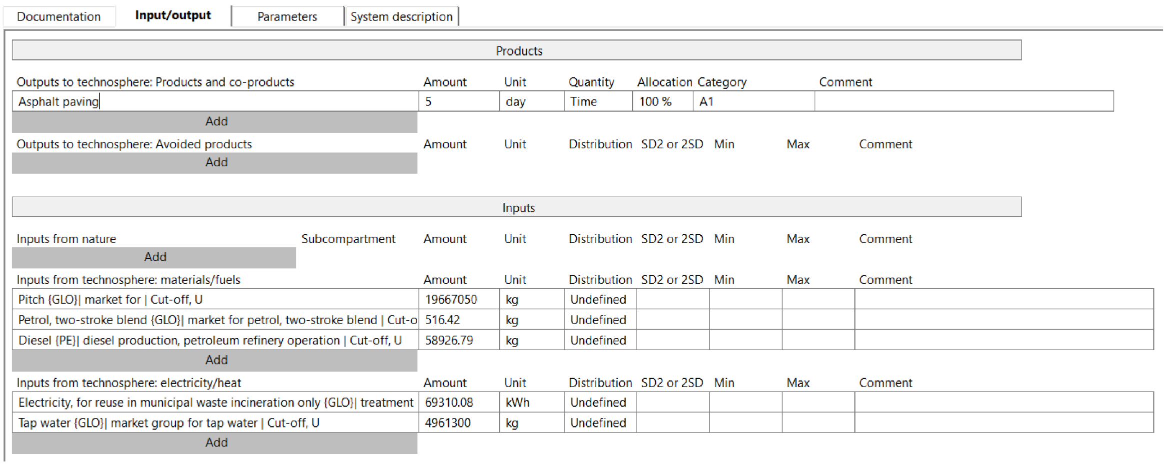

Figure 9. Calculated inputs for asphalt paving.

3.2. Regression Prediction of Carbon Emissions Based on GA-BPNN

3.2.1. Prediction Model Selection

The BPNN is a multilayer feedforward neural network that employs the error backpropagation algorithm for training. This process utilizes the gradient descent method along with backpropagation to iteratively adjust the network's weights and thresholds. The feedforward neural network is designed to minimize the sum of squared errors, demonstrating strong learning capabilities and effective data processing, making it suitable for predicting carbon emissions in this study.

However, the initial weights and thresholds of BPNNs are typically generated through overly randomized functions, meaning that the training process heavily relies on the error function to adjust these randomly assigned values. If the initial weights and thresholds are not optimally chosen, they can adversely affect the results, leading to unstable predictive accuracy. Furthermore, the gradient descent method is prone to local optima, which may prevent the identification of the best weights and thresholds. Consequently, it is imperative to implement a suitable optimization strategy for selecting weights and thresholds during the BPNN training process to mitigate the risk of converging on local optimum solutions.

In this study, the GA-BPNN is introduced as a hybrid training method that integrates genetic algorithms with the backpropagation algorithm. The GA encodes the problem parameters as chromosomes and employs iterative operations while simulating the natural selection and genetic mechanisms of Darwinian evolution to facilitate the exchange of chromosome information within the population. This approach generates solutions that align with optimization objectives. By incorporating optimal weights and thresholds into the neural network model, the BPNN is able to compute the outputs of individual neurons through forward propagation. Subsequently, the weights and thresholds of each neuron are adjusted using the error backpropagation algorithm until the overall error is minimized. This method enhances the model's ability to fit training data while ensuring generalization to testing data.

To demonstrate the superiority of the GA-BPNN model, this study also incorporates the Support Vector Regression (SVR) for comparative analysis. The SVR prediction framework primarily utilizes concepts of dimensionality enhancement and linearization to achieve optimal predictions. Moreover, the SVR model effectively circumvents issues associated with local minima, overfitting, and underfitting that may arise in other machine learning techniques, rendering it particularly suitable for small sample sizes and non-linear regression challenges. In this study, 100 small sample datasets are selected for prediction, highlighting the high applicability of the SVR model.

3.2.2. Modeling Process

(1) Datasets

A total of 100 valid samples were constructed for model training and testing. These samples were synthesized based on field monitoring records, measured construction parameters, and calibrated simulation results from the professional carbon emission calculation software. Each sample corresponds to a realistic construction scenario with reasonable variations in construction intensity, transportation organization, equipment working conditions, on-site operation configuration, and ventilation duration, leading to a certain degree of discreteness that enhances the representativeness and generalization potential of the dataset. The input variables include asphalt production, gasoline consumption, diesel consumption, electricity consumption, and tap water consumption, while the output variable is the total carbon emission obtained from the HLCA calculation. Prior to model training, all input variables were normalized to the range of [0, 1] using min–max scaling to eliminate dimensional differences and improve convergence efficiency. The dataset was randomly divided into a training set (80%) and a testing set (20%) to ensure reliable and repeatable model evaluation.

The distribution of data within the training and testing set samples of this model dataset is illustrated in Figure 10.

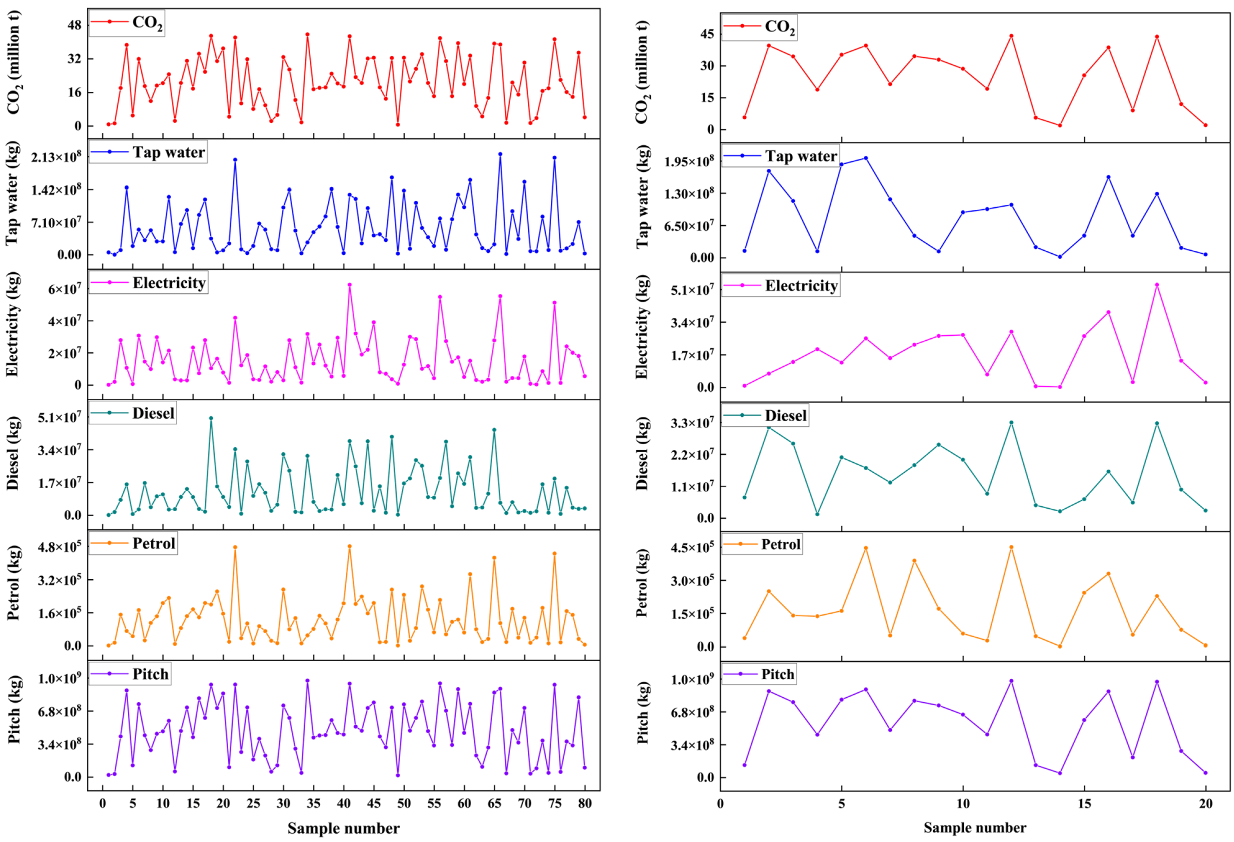

(**a**) (**b**)

Figure 10. Model dataset: (**a**) training set; (**b**) testing set.

As illustrated in Figure 10, the statistical distributions of the five input variables (i.e., asphalt output, petrol consumption, diesel consumption, electricity consumption, and tap water consumption) and the output carbon emission variable are clearly displayed for both the training and testing subsets. The figure shows that the samples in both subsets cover reasonable fluctuation ranges and exhibit acceptable data dispersion, which are consistent with actual engineering characteristics of long tunnel asphalt pavement construction. The training and testing sets follow similar distribution patterns, ensuring that the testing set can effectively verify the generalization ability of the trained models. The overall data distribution further confirms the representativeness and reliability of the established dataset for carbon emission prediction.

(2) Optimization of model parameters

The network structure of the BPNN is determined as 5-10-1 according to the empirical formula and trial comparisons. Key parameters of the GA-BPNN model are set based on mature empirical ranges in machine learning literature and multiple pre-experimental comparisons. A population size of 20 is a typical and effective setting for small-sample engineering prediction problems, and it can ensure population diversity while avoiding excessive computation and slow convergence. A moderate crossover probability of 0.5 is adopted, which is within the commonly used range of 0.4–0.7 in genetic algorithms. It balances inheritance and variation effectively; a small mutation probability of 0.05 is used (within the conventional range of 0.01–0.1), which prevents the loss of excellent individuals while avoiding random search; the number of evolutionary generations is set to 30 based on iteration curves. The fitness tends to be stable at approximately 19 generations, and 30 generations can fully guarantee convergence. A small learning rate of 0.01 is used to ensure stable convergence and prevent large fluctuations during training. The final parameter values are listed in Table 2, which have been verified to provide stable convergence, high predictive accuracy, and good generalization through repeated tests.

Table 2. GA-BPNN parameters.

Population Size	**Crossover Probability**	**Probability of Mutation**	**Hereditary Number**	**Maximum Number of Training Sessions**	**Learning Rate**	**Error Threshold**
20	0.5	0.05	30	1000	0.01	1×10^{-6}

(3) Model Evaluation

The parameters were brought into the GA-BPNN prediction model for CO_2 emissions prediction using Matlab (2018b) software. To evaluate and compare the prediction models systematically, two complemental assessment frameworks are executed in this study.

The physical error framework employs Mean Absolute Error (MAE), Mean Bias Error (MBE), and Root Mean Square Error (RMSE) to capture absolute variations in physical carbon emissions (expressed in t CO_2). The dimensionless trajectory framework utilizes the Mean Squared Error (MSE), Coefficient of Determination (R^2), Mean Absolute Percentage Error (MAPE), Theil Inequality Coefficient (TIC), and Directional Accuracy (DA). Specifically, the Mean Squared Error is the exact square of the Root Mean Square Error ($\text{MSE} = \text{RMSE}^2$). While the physical metrics reflect the absolute magnitude of carbon emission discrepancies, the dimensionless parameters evaluate global fitting quality (R^2), relative point-by-point errors (MAPE), prediction envelope closeness (TIC), and directional synchronization (DA).

The value of MSE is in the range of [0, +∞), which is equal to 0 when the predicted value coincides exactly with the real value. The smaller the value, the smaller the error. The calculation formula is as follows:

$$MSE = \frac{1}{l}\sum_{i=1}^{l}(\hat{y}_i - y_i)^2 \quad (17)$$

R^2 denotes the proportion of variation in the dependent variable that is explained by the independent variable through the regression relationship, with a value in the range of [0, 1]. The higher the value, the better the model's performance. The calculation formula is as follows:

$$R^2 = \frac{\left(l\sum_{i=1}^{l}\hat{y}_i y_i - \sum_{i=1}^{l}\hat{y}_i\sum_{i=1}^{l}y_i\right)^2}{\left(l\sum_{i=1}^{l}\hat{y}_i^2 - \left(\sum_{i=1}^{l}\hat{y}_i\right)^2\right)\left(l\sum_{i=1}^{l}{y_i}^2 - \left(\sum_{i=1}^{l}y_i\right)^2\right)} \quad (18)$$

The advantage of MAPE is mainly that it does not change with the scaling of the dependent variable. The smaller the value, the smaller the error, the better the regression of the model, and the higher the predictive accuracy. The calculation formula is as follows:

$$MAPE = \frac{100\%}{l}\sum_{i=1}^{l}\left|\frac{\hat{y}_i - y_i}{y_i}\right| \quad (19)$$

The value range of TIC is [0, 1]. The smaller its value, which indicates a smaller error between the predicted value and the real value, the higher the predictive accuracy. The calculation formula is as follows:

$$TIC = \frac{\sqrt{\frac{1}{l}\sum_{i=1}^{l}(\hat{y}_i - y_i)^2}}{\sqrt{\frac{1}{l}\sum_{i=1}^{l}(\hat{y}_i)^2} + \sqrt{\frac{1}{l}\sum_{i=1}^{l}(y_i)^2}} \quad (20)$$

DA is used to judge whether the direction of change of the predicted value and the real value compared to the previous period is the same, and the closer its value is to 1, the higher the accuracy of the model prediction. The formula is as follows:

$$\begin{cases} DA = \frac{1}{l}\sum_{i=1}^{l}A_i \\ A_i = \begin{cases} 1\ (\hat{y}_{i+1} - \hat{y}_i)(y_{i+1} - y_i) > 0 \\ 0\ (\hat{y}_{i+1} - \hat{y}_i)(y_{i+1} - y_i) \le 0 \end{cases} \end{cases} \quad (21)$$

where l is the number of samples in the testing set. y_i (i = 1, 2, . . ., l) is the true value of the ith sample. $\hat{y}_i$ (i = 1, 2, . . ., l) is the ith sample predicted value.

In addition, four evaluation parameters were utilized as the physical error framework: the coefficient of determination (R^2), the mean absolute error (MAE), the mean bias error (MBE), and the root mean square error (RMSE). These parameters were employed to assess the performance of the model prediction results. The calculation formulas for these metrics are as follows:

$$\begin{cases} MAE = \frac{1}{n}\sum_{i=1}^{n}|y_i - \hat{y}_i| \\ MBE = \frac{1}{n}\sum_{i=1}^{n}(y_i - \hat{y}_i) \\ RMSE = \sqrt{\frac{1}{n}\sum_{i=1}^{n}(y_i - \hat{y}_i)^2} \end{cases} \quad (22)$$

3.2.3. Prevention of Overfitting and Stability Evaluation

Given the relatively compact sample size of the dataset (100 samples), preventing overfitting and ensuring prediction stability are paramount for the machine learning model. Three specific regularizations were implemented:

Five-Fold Cross-Validation: The 100 samples were partitioned using a five-fold cross-validation method. In each fold, 80% of the data (80 samples) was allocated for training and optimization, while the remaining 20% (20 samples) served as a blind testing set. This process was repeated 5 times, ensuring that the model's performance was evaluated across the entire dataset without selection bias. Network Topology Constraint: A single-hidden-layer architecture ($5 \times 10 \times 1$) was selected. Limiting the number of hidden neurons to 10 restricts the hypothesis space of the neural network, effectively preventing the network from "memorizing" noise in the training data (overfitting). Early Stopping: An early stopping threshold of six epochs was applied during the backpropagation training phase. If the validation loss failed to decrease for six consecutive iterations, training was immediately terminated. To quantitatively evaluate the generalization capability, the performance of the GA-BPNN was contrasted between the training and testing phases. The model achieved a high R^2 of 0.9506 on the training set and maintained an R^2 of 0.9881 on the testing set. The minimal discrepancy between the training and testing performance, coupled with a low Mean Absolute Percentage Error (MAPE) of 22.8997%, strongly demonstrates that the model possesses excellent stability and is free of significant overfitting.

3.2.4. Projected Results and Evaluation

(1) Model prediction results

This study develops a carbon emission prediction model using 100 samples shown in Figure 10, which are divided into 80 training samples and 20 testing samples. As illustrated in Figure 11, the fitness curve of the GA-BPNN declines rapidly in early generations and stabilizes after about 19 generations, indicating that the genetic algorithm has converged to a near-optimal set of initial weights and thresholds. These optimized parameters are then decoded and applied to initialize the BPNN for formal training.

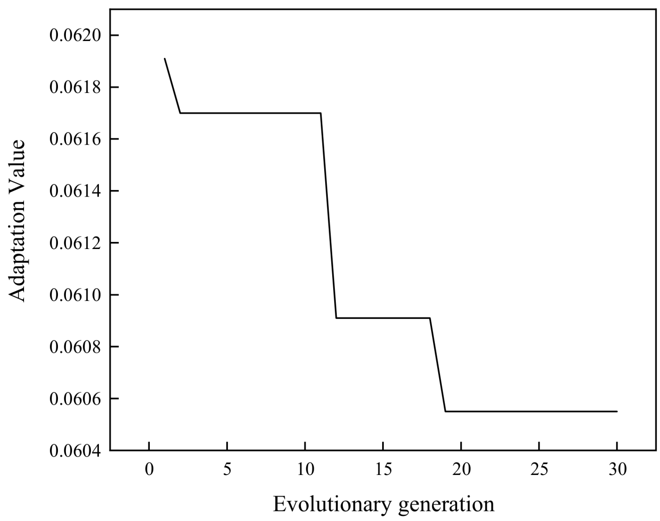

Figure 11. GA-BPNN fitness curve plot.

Using Matlab (2018b) software, the GA-BPNN prediction model was built and predicted. The prediction results are shown in Figure 12, and the R^2, MAE, MBE, and RMSE of the training set of the prediction model are 0.9506, 1.3447, 0.3934, and 2.7466, respectively, and those of the testing set are 0.9881, 1.2758, 0.8559, and 1.5457, respectively. It can be seen that the model has a strong learning ability and high predictive accuracy.

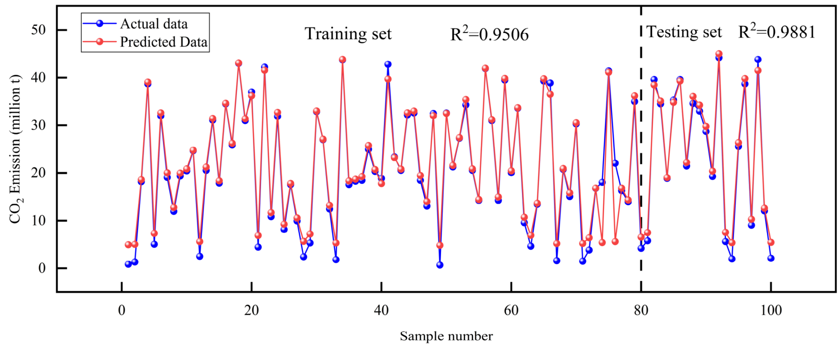

Figure 12. GA-BPNN model prediction results.

To comprehensively compare the variance between the actual and predicted values generated by the model, error statistics for both the training and testing sets are presented in Figure 13. The Figure 13a illustrates that the predicted value errors within the training set data predominantly fall within the 20% margin, with some data exhibiting predicted value errors greater than 40%. Conversely, Figure 13b demonstrates that the predicted value errors within the testing set data mostly lie within the 20% range, with only two data points showing prediction value errors greater than 40%. This observation highlights the high predictive accuracy of the GA-BPNN model that has been developed.

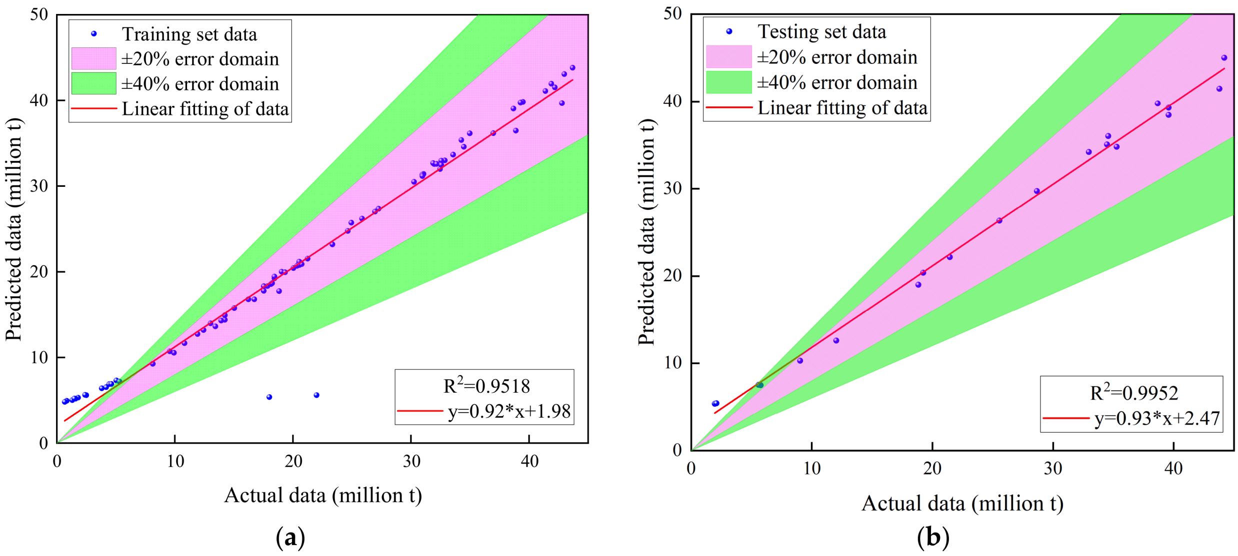

Figure 13. Calculated results of GA-BPNN prediction error: (**a**) training set; (**b**) testing set (The "*" means a multiplication sign).

(2) Evaluation of forecast results

To analyze the performance of the developed GA-BPNN prediction model, the prediction of CO_2 emissions was tested with the traditional support vector machine model and the BPNN model. Using the data in Figure 10 as sample data, the SVR and BPNN prediction models were built using Matlab (2018b) software. The model parameters are shown in Tables 3 and 4.

Table 3. BPNN parameters.

Network Structure	Training Function	Learning Rate	Maximum Epochs	Error Threshold
5-10-1	trainlm	0.01	1000	1×10^{-6}

Table 4. SVR parameters.

Kernel Function	Kernel Parameter Gamma	Penalty Parameter C	Epsilon	Solver
RBF kernel	0.1	1	0.1	SMO

The prediction of CO_2 emissions was carried out, and the prediction results of different models are shown in Figure 14. Among them, the R^2, MAE, MBE, and RMSE of the training set of the SVR prediction model were 0.9286, 1.9261, −0.8116, and 3.3009, respectively; the R^2, MAE, MBE, and RMSE of the testing set were 0.9876, 1.4511, −0.6033, and 1.5771, respectively. The R^2, MAE, MBE, and RMSE of the training set of the BPNN prediction model are 0.9428, 1.4156, −0.0929, and 2.9548, respectively; and the R^2, MAE, MBE, and RMSE of the testing set are 0.9743, 1.6489, −0.4829, and 2.2677, respectively. It can be seen that the SVR and BPNN models also have high prediction accuracies of CO_2 emissions, but the accuracies are not as high as those of the GA-BPNN model.

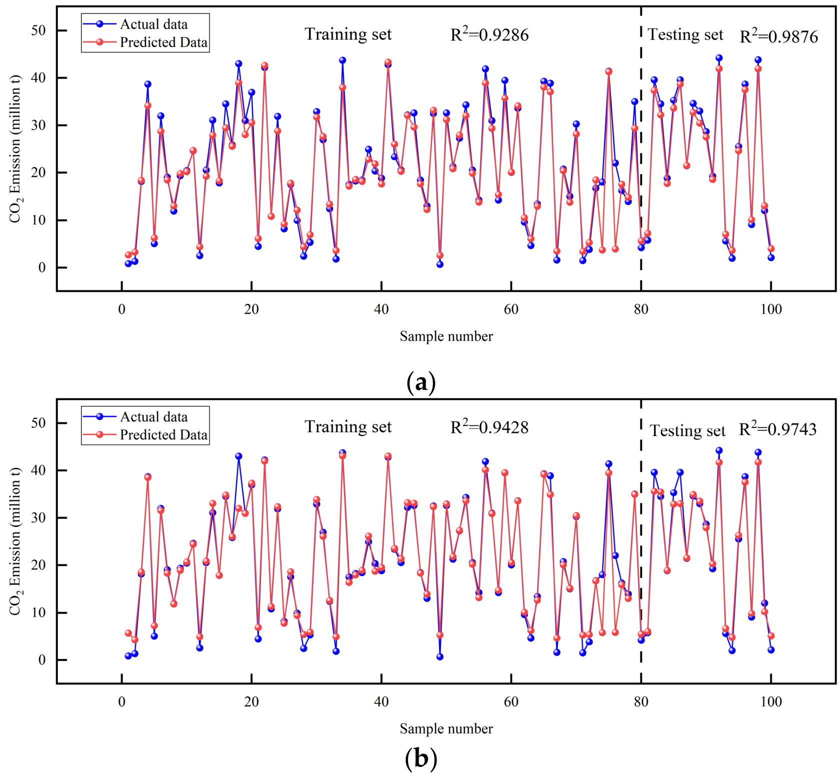

Figure 14. Prediction results of different prediction models: (**a**) SVR prediction results; (**b**) BPNN prediction results.

The performance of each model is further evaluated using the model evaluation metrics. The evaluation metrics settlement results for the model training and testing sets are shown in Table 5, and the corresponding model performance evaluation radar diagram is shown in Figure 15.

Table 5. Calculated results of the model performance assessment.

Sample Set	Evaluation Indicators	GA-BPNN	SVR	BPNN
Training set	MSE	7.5440	10.8959	8.7308
	R^2	0.9506	0.9286	0.9428
	MAPE	36.8253%	23.6385%	35.8835%
	TIC	0.0559	0.0690	0.0607
	DA	0.9750	0.9500	0.9357
Testing set	MSE	2.3890	2.4873	5.1426
	R^2	0.9881	0.9876	0.9743
	MAPE	22.8997%	15.3175%	19.8931%
	TIC	0.0270	0.0283	0.0407
	DA	1.0000	1.0000	1.0000

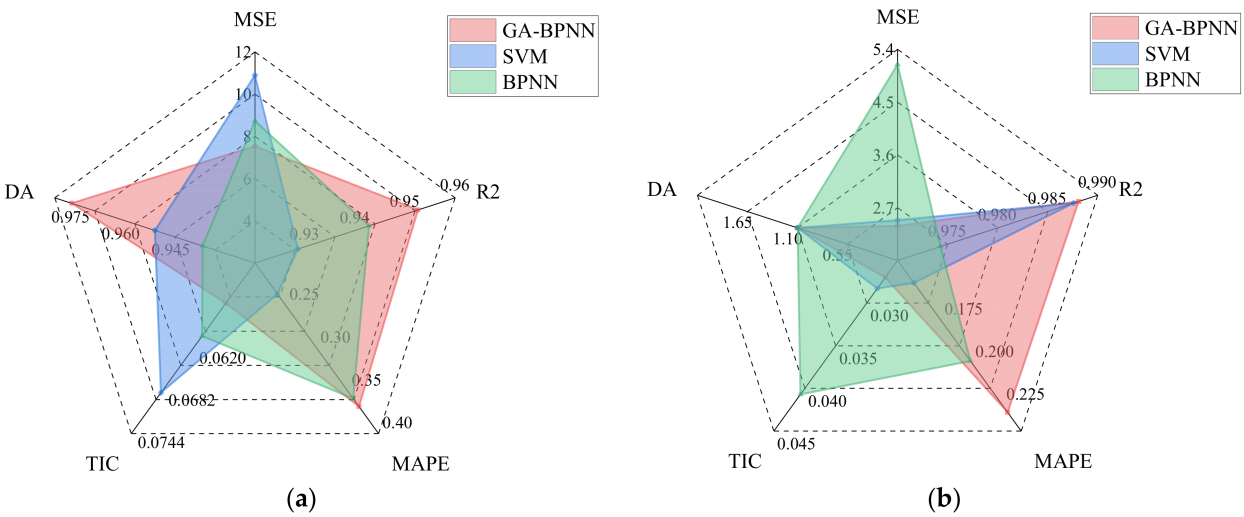

Figure 15. Radar plot for performance evaluation of different predictive models: (**a**) training set; (**b**) testing set.

As shown in Table 5 and Figure 15, the GA-BPNN model achieves the highest R^2 (0.9881), the lowest MSE (2.3890), the lowest TIC (0.0270), and DA = 1.000 on the testing set, indicating the strongest global fitting accuracy, minimal overall error, highest prediction stability, and fully consistent trend prediction. These indexes dominate the comprehensive judgment of model performance. Although the MAPE value of GA-BPNN is slightly higher than that of SVR, this phenomenon is mainly caused by individual sample fluctuation in the small-sample dataset (100 groups). MAPE is highly sensitive to extreme points and abnormal deviations of individual samples, which cannot represent the global predictive accuracy of the model. In contrast, the other four indicators reflect the overall prediction capability more stably and reliably. Therefore, based on a comprehensive quantitative evaluation of global error, fitting effect, stability, and trend consistency, the GA-BPNN model exhibits better overall performance and higher stability in carbon emission prediction of long tunnel asphalt pavement construction. It is therefore considered more suitable for the engineering scenario in this study.

4. Discussion

This study integrates pertinent theoretical methodologies with the practical context of the project to investigate the calculation and prediction techniques for carbon emissions arising from asphalt paving construction within long tunnels. It establishes an HLCA-based carbon emission accounting model and a GA-BPNN-based prediction model, both of which demonstrate good applicability to engineering practice. The calculation and prediction outcomes demonstrate high precision and substantial guiding implications, offering valuable insights for carbon emission management, decision-making processes, and swift carbon emission forecasts during the specialized construction of asphalt paving in extended tunnels.

The carbon emission intensity of asphalt pavement construction in long tunnels ranges from 18.2 to 21.8 kg CO_2-eq/m^2, which is significantly higher than that of conventional open-road pavement construction. This gap arises mainly from two unique characteristics of long tunnel environments: continuous high-power mechanical ventilation must be equipped to ensure construction safety, making ventilation electricity consumption an important emission component; and the narrow and confined space restricts construction and transportation efficiency, leading to increased machine idling time and additional fuel consumption. Nevertheless, asphalt mixture production and heating processes still contribute more than 80% of total carbon emissions, representing the dominant carbon hotspot throughout the construction stage. Therefore, reducing energy consumption in material heating and mixing remains the most critical measure for carbon reduction in tunnel asphalt pavement construction.

Among the four construction schemes, Option 2 achieves the optimal low-carbon performance by reasonably configuring mixing plant capacity and optimizing logistics organization. This scheme realizes stable carbon reduction purely through process coordination and management optimization, without changing asphalt materials or affecting pavement mechanical performance. Although material-improving technologies also have carbon reduction effects, their applications in long tunnels are limited by high humidity, low temperature, and strict pavement safety standards. In contrast, organizational and logistical optimization is more adaptable and easier to implement, making it a feasible and reliable low-carbon strategy for tunnel asphalt pavement projects.

In this study, three machine learning algorithms (GA-BPNN, BPNN, and SVR) were compared to evaluate their efficacy in predicting construction-phase carbon emissions. The comparative analysis reveals that the hybrid GA-BPNN model exhibits superior predictive capability and generalization performance.

As presented in Table 5, the GA-BPNN model achieved a high coefficient of determination ($R^2 = 0.9881$) on the testing dataset. In contrast, the standard BPNN and SVR models achieved lower R^2 values of 0.9743 and 0.9876, respectively. The performance gap between GA-BPNN and the standard BPNN primarily stems from the optimization of initial network parameters. Standard BPNN models rely on random weight and bias initialization, which frequently leads the gradient descent algorithm to trap in local minima, causing suboptimal convergence and poor generalization. By integrating the Genetic Algorithm (GA), the parameter space is globally searched and optimized before training. This hybrid approach establishes a robust initial network structure (5-10-1), ensuring rapid convergence around the 19th generation and a significantly lower testing Mean Squared Error ($MSE = 2.3890$) compared to the standard BPNN ($MSE = 5.1426$).

Furthermore, Support Vector Regression (SVR) is highly effective for processing low-dimensional datasets; its performance ($R^2 = 0.9876$, $MSE = 2.4873$) is limited when handling the highly non-linear, multi-variable features inherent in tunnel asphalt construction. Factors such as material transport distances, mixing temperatures, and equipment scheduling create highly complex, non-linear relationships with carbon emissions. SVR struggles to map these complex feature interactions using static kernel functions. Furthermore, civil engineering carbon emission datasets are often small due to the high cost of data collection. Standard deep learning architectures require thousands of samples to avoid overfitting. Furthermore, the GA-BPNN model demonstrated excellent generalization and stability with a compact dataset of 100 samples. Unlike models that rely on actual post-construction energy consumption logs, this model uses five macroscopic, pre-construction parameters easily obtained from design documents. This enables rapid, reliable ex ante carbon forecasting during the bidding and planning phases of tunnel pavement projects.

While this study has made initial strides in exploring the calculation and prediction methodologies for carbon emissions in long tunnel asphalt paving construction, several challenges warrant further investigation due to the intricate nature of asphalt paving in long tunnels, data compilation complexities, and the evolving landscape of carbon emission research. The following issues merit deeper scrutiny:

(1) Enhancing Carbon Emission Calculation Methods during Operation and Maintenance Phases: The current HLCA model primarily focuses on the construction phase, leading to disparities in carbon emission calculations across operation and maintenance stages due to temporal, spatial, and personnel variations. Diverse geographical factors, technical proficiency, management standards, regional topography, geological structures, and climatic nuances influence carbon emissions in asphalt paving construction across different regions of extended tunnels. None of the literature [40,41] considered the carbon emissions during the later operation and maintenance period, whereas the literature [42] considered the environmental impact of pavement preservation work, maintenance activities, etc., during the use phase. The presence of systematic and incidental errors underscores the need to refine existing carbon emission calculation methodologies to encompass operation and maintenance periods comprehensively.

(2) Optimizing Input Parameters in the GA-BPNN Prediction Model: The proposed GA-BPNN model is intended primarily for rapid estimation during the construction execution stage, when key consumption data can be collected from field logs and operational records. Rather than replacing the HLCA accounting framework, it serves as a data-driven supplementary tool for efficient carbon-emission estimation and management. Previous studies have employed various prediction models with distinct input variables, ranging from energy consumption to industrial activities, to anticipate carbon emissions across different sectors [43–45]. Aligning with the input parameters utilized in prior research, it is imperative to streamline the input variables in the GA-BPNN model, collate a substantial dataset of carbon emission data from real-world projects, and refine the prediction model accordingly.

5. Conclusions

This study delves into precise carbon emission calculations stemming from asphalt paving construction in long tunnels, employing the HLCA framework. Additionally, it explores carbon emission prediction methods using pertinent data, culminating in the development of corresponding models. The key findings are outlined as follows:

(1) HLCA-Based Carbon Emission Calculation Model for Long Tunnel Asphalt Pavement Construction: Grounded in HLCA theory, this model dissects the carbon emission dynamics across five stages of asphalt paving in extended tunnels. Encompassing the entire construction process, with a particular emphasis on refining carbon emissions during asphalt mixing plant operations, this model provides a robust and feasible accounting framework. And the accuracy of the carbon emission calculations has been validated through computational software.

(2) Comparative Analysis of Carbon Emissions in Long Tunnel Asphalt Paving Options: Evaluation of various construction options on the entire tunnel functional unit reveals that Option 2 boasts the lowest carbon emissions, aligns with construction timelines, and entails minimal investment in asphalt mixing plant construction and operation. This optimal construction choice not only guides carbon emission control and reduction strategies but also serves as a blueprint for achieving emission reduction objectives effectively.

(3) GA-BPNN-Based Carbon Emission Prediction Model: The developed prediction model, based on GA-BPNN, showcases superior predictive accuracy when contrasted with traditional SVR and BPNN models. This effective prediction model holds promise for accurate carbon emission forecasts in asphalt paving construction scenarios.

Author Contributions: Data curation, D.Y.; formal analysis, D.L. and D.Y.; methodology, D.L. and J.W.; supervision, J.W. and Q.S.; validation, Q.S.; and writing original draft, D.Y. All authors have read and agreed to the published version of the manuscript.

Funding: This research received no external funding.

Data Availability Statement: The original contributions presented in this study are included in the article. Further inquiries can be directed to the corresponding author.

Acknowledgments: The authors would like to thank Road & Bridge South China Engineering Co., Ltd., for their assistance with conducting the monitoring of data.

Conflicts of Interest: The authors, Q.S. and J.W., are employed by the company Road & Bridge South China Engineering Co., Ltd. The remaining authors declare that the research was conducted in the absence of any commercial or financial relationships that could be construed as potential conflicts of interest.

Appendix A. Tables of Option Statistics

Table A1. Carbon emission factors of major power grids in China.

Name	Carbon Emission Factor (kg CO_2/kWh)	Electricity Tariff (Yuan/kWh)	Carbon Emission Factor (kg CO_2/Yuan)	Source
North China Regional Power Grid	0.8843	0.0071	124.55	Reference [39]
East China Regional Power Grid	0.7035	0.0095	74.05	
Northeast Regional Power Grid	0.7769	0.0087	89.30	
Central China Regional Power Grid	0.5257	0.0100	52.57	
Northwest Regional Power Grid	0.6671	0.0200	33.36	
Southern Regional Power Grid	0.5271	0.0471	11.19	

Note. The transmission price of the southern regional power grid is calculated by using a gradient according to different provinces, and the tunnel in this paper is located in Guangxi Province, i.e., the transmission and distribution price of the Guangxi power grid is used.

Table A2. Carbon emission factors for fossil fuels.

Categorization	Fossil Fuel Type	Carbon Emission Factor (kg CO_2/kg)	Unit Price of Fuel (Yuan/kg)	Carbon Emission Factor (kg CO_2/Yuan)	Source
liquid fuel	fuel oil	3.74	5.28	0.71	References [39,46]
	petrol	3.50	10.81	0.32	
	diesel	3.67	7.56	0.49	
	General Kerosene	3.26	4.40	0.82	
solid fuel	ferroalloys	2.35	2.53	0.93	
	coking coal	2.94	2.26	1.30	
gas fuel	petroleum	2.36	5.00	0.47	

Table A3. Carbon Emission Factor for Construction and Operation of Asphalt Mixing Plant.

Point	Input Costs (Yuan/t/km)	Carbon Emission Factor (kg CO_2/Yuan)	Source
Construction of an asphalt mixing plant	0.83	0.81	References [33,47,48]
Asphalt mixing plant operations	0.27	1.2	

Table A4. Carbon emission factors for manual consumption.

Name	Carbon Emissions (kg CO_2/Person/Day)	Average Wage of Manpower (Yuan/Day)	Carbon Emission Factor (kg CO_2/Yuan)	Source
Labor	6.61	216.80	0.03	Reference [49]

Note. In this study, the labor emission coefficients reflect not only the physical metabolic rate of workers during tunnel construction but also the per capita daily energy consumption of the construction camp (electricity, domestic water, and cooking fuels). These parameters were calibrated using the "General Principles for Calculation of Total Production Energy Consumption (GB/T 2589-2020 [50])" combined with prior empirical measurements in Chinese infrastructure projects (Reference [49]).

Appendix B. IOA Carbon Emission Factors

Table A5. Carbon emission factors for asphalt mixing plants with different production capacities.

Asphalt Mixing Plant Capacity (t/h)	Energy Use		Carbon Emission Factor (kg CO_2/Shift)	Source
	Heavy Oil (kg)	Electricity (kWh)		
30	897.60	624.02	3622.24	References [39,51]
60	1795.20	1618.42	7439.19	
120	5170.18	1618.42	19,825.36	
160	6893.57	2620.88	26,677.20	
240	10,340.35	3895.09	39,996.73	
320	13,787.14	5151.17	53,306.77	
380	16,372.22	6111.36	63,298.79	

Table A6. Carbon emissions from asphalt transportation per unit volume (1000 m^3).

Maximum Transportation Capacity of Dump Trucks (t)	Consumption per Shift (kg)	First 1 km of Shift	Carbon Emissions from the First 1 km	Number of Shifts per 0.5 km of Additional Transportation	Carbon Emissions per 0.5 km of Additional Transportation	Source
10	55.32	9.79	1689.75	0.85	146.71	References [39,51]
12	61.60	8.22	1579.80	0.74	142.22	
15	67.89	6.91	1463.68	0.58	122.85	
20	72.92	5.14	1282.84	0.41	93.28	

Table A7. Carbon emissions per unit volume of asphalt paving (1000 m^3).

Asphalt Mixing Plant Capacity (t/h)	Type of Paver	Number of Shifts	Diesel Fuel Consumption per Shift	CO_2 Emissions (kg)	Source
30	4.5 m	10.77	42.06	1662.46	References [39,51]
60	4.5 m	7.53	42.06	1162.33	
120	6.0 m	4.07	46.63	696.51	
160	9.0 m	2.87	96.00	1011.16	
240	12.5 m	1.92	136.23	959.93	
320	12.5 m	1.46	136.23	729.95	
380	12.5 m	1.39	136.23	694.95	

Table A8. Carbon emissions per unit volume of asphalt milling (1000 m^3).

Asphalt Mixing Plant Capacity (t/h)	Types of Road Rollers	Number of Shifts	Diesel Fuel Consumption per Shift	CO_2 Emissions (kg)	Total CO_2 Emissions
30	Vibratory roller (10 t) Tire rollers (9~16 t)	19.38 9.70	54.40 33.60	1054.27 325.92	1380.19
60	Vibratory roller (10 t) Tire rollers (9~16 t) Tire rollers (16~20 t)	13.56 6.78 5.78	54.40 33.60 42.40	737.66 227.81 245.07	1210.54
120	Vibratory roller (10 t) Tire rollers (16~20 t) Tire rollers (20~25 t)	11.52 5.48 2.34	54.40 42.40 50.40	626.69 232.35 117.94	976.98
160	Vibratory roller (10 t) Tire rollers (16~20 t) Tire rollers (20~25 t)	10.84 2.2 2.32	54.40 42.40 50.40	589.70 93.28 116.93	799.91
240	Vibratory roller(15 t) Tire rollers (16~20 t) Tire rollers (20~25 t)	5.38 2.68 2.58	80.80 42.40 50.40	434.70 113.63 130.03	678.36
320	Vibratory roller (15 t) Tire rollers (16~20 t) Tire rollers (20~25 t)	6.14 2.04 3.92	80.80 42.40 50.40	496.11 86.50 197.59	780.20
380	Vibratory roller (15 t) Tire rollers (16~20 t)	7.00 1.64	80.80 42.40	565.60 69.54	635.14

Table A9. Tunnel Ventilation Carbon Emissions.

Equipment Name	Power (Output)	Electricity Consumption (kWh/Shift/h)	CO_2 Emissions (kg/Shift/h)
Press-in ventilator	110 kW	110	58

Appendix C. Carbon Emissions from Asphalt Construction Machinery

Table A10. Option 1.

Serial Number	Equipment Name	Specification	Quantities	Consume
1	Asphalt mixing plant	240 t/h	1	Construction: 15 million yuan Operation: 5 shifts Labor: 19
2	Asphalt transporter	12 t	8	410 km/car Labor: 10
3	Three-roller paver	12.5 m	1	Labor: 2
4 5 6	Tire Roller Vibratory Road Roller Tire Roller	20~25 t 15 t 16~20 t	1 1 1	Labor: 5
7	Press-in ventilator	110 kW	2	5 shifts

Table A11. Option 2.

Serial Number	Equipment Name	Specification	Quantities	Consume
1	Asphalt mixing plant	120 t/h	2	Construction: 12 million yuan Operation: 5 shifts Labor: 26
2	Asphalt transporter	12 t	8	410 km/car Labor: 10

Table A11. *Cont.*

Serial Number	Equipment Name	Specification	Quantities	Consume
3	Three-roller paver	12.5 m	1	Labor: 2
4 5 6	Tire Roller Vibratory Road Roller Tire Roller	20~25 t 15 t 16~20 t	1 1 1	Labor: 5
7	Press-in ventilator	110 kW	2	5 shifts

Table A12. Option 3.

Serial Number	Equipment Name	Specification	Quantities	Consume
1	Asphalt mixing plant	120 t/h 60 t/h	1 2	Construction: 13.2 million yuan Operation: 5 shifts Labor: 29
2	Asphalt transporter	12 t	8	410 km/car Labor: 10
3	Three-roller paver	12.5 m	1	Labor: 2
4 5 6	Tire Roller Vibratory Road Roller Tire Roller	20~25 t 15 t 16~20 t	1 1 1	Labor: 5
7	Press-in ventilator	110 kW	2	5 shifts

Table A13. Option 4.

Serial Number	Equipment Name	Specification	Quantities	Consume
1	Asphalt mixing plant	120 t/h 30 t/h	1 4	Construction: 13.2 million yuan Operation: 5 shifts Labor: 37
2	Asphalt transporter	12 t	8	410 km/car Labor: 10
3	Three-roller paver	12.5 m	1	Labor: 2
4 5 6	Tire Roller Vibratory Road Roller Tire Roller	20~25 t 15 t 16~20 t	1 1 1	Labor: 5
7	Press-in ventilator	110 kW	2	5 shifts

Appendix D. Detailed Step-by-Step Numerical Calculations of HLCA

(1) CO_2 emissions from production processes:

Using computational software, the CO_2 emissions from asphalt production were calculated to be 8,340,000 kg. Referring to Appendix A and Tables A7–A9, the calculations are as follows:

Option 1: The CO_2 emissions from the construction and operation of the asphalt mixing plant are 12,349,983.6 kg; the CO_2 emissions from labor consumption are 617.88 kg. The calculation formulas are as follows:

$$0.81\ \mathrm{kg/yuan} \times 15,000,000\ \mathrm{yuan} + 1 \times 39,996.73\ \mathrm{kg/shift} \times 5\ \mathrm{shifts} = 12,349,983.65\ \mathrm{kg} \tag{A1}$$

$$0.03\ \mathrm{kg/yuan} \times 19 \times 216.8\ \mathrm{yuan/d} \times 5\ \mathrm{d} = 617.88\ \mathrm{kg} \tag{A2}$$

Option 2: The CO_2 emissions from the construction and operation of the asphalt mixing plant are 9,918,253.6 kg; the CO_2 emissions from labor consumption are 845.52 kg. The calculation formulas are as follows:

$$0.81\ \text{kg/yuan} \times 12,000,000\ \text{yuan} + 2 \times 19,825.36\ \text{kg/shift} \times 5\ \text{shifts} = 9,918,253.6\ \text{kg} \tag{A3}$$

$$0.03\ \text{kg/yuan} \times 26 \times 216.8\ \text{yuan/d} \times 5\ \text{d} = 845.52\ \text{kg} \tag{A4}$$

Option 3: The CO_2 emissions from the construction and operation of the asphalt mixing plant are 10,865,518.7 kg; the CO_2 emissions from labor consumption are 943.08 kg. The calculation formulas are as follows:

$$\frac{0.81\ \text{kg}}{\text{yuan}} \times 13,200,000\ \text{yuan} + 1 \times \frac{19,825.36\ \text{kg}}{\text{shift}} \times 5\ \text{shifts} + 2 \times 7439.19\ \text{kg/shift} \times 5\ \text{shifts} = 10,865,518.70\ \text{kg} \tag{A5}$$

$$0.03\ \text{kg/yuan} \times 29 \times 216.8\ \text{yuan/d} \times 5\ \text{d} = 943.08\ \text{kg} \tag{A6}$$

Option 4: The CO_2 emissions from the construction and operation of the asphalt mixing plant are 10,863,571.6 kg; the CO_2 emissions from labor consumption are 1203.24 kg. The calculation formulas are as follows:

$$\frac{0.81\ \text{kg}}{\text{yuan}} \times 13,200,000\ \text{yuan} + 1 \times \frac{19,825.36\ \text{kg}}{\text{shift}} \times 5\ \text{shifts} + 4 \times \frac{3622.24\ \text{kg}}{\text{shift}} \times 5\ \text{shifts} = 10,863,571.60\text{kg} \tag{A7}$$

$$0.03\ \text{kg/yuan} \times 37 \times 216.8\ \text{yuan/d} \times 5\ \text{d} = 1203.24\ \text{kg} \tag{A8}$$

(2) CO_2 emissions from transportation:

The total asphalt production capacity of all four options is 240 t/h, so the CO_2 emissions from the transportation process are also used in the same way. Referring to Appendix A and Tables A8 and A10, the calculations are as follows.

CO_2 emissions from transportation: 19,208.27 kg; CO_2 emissions from labor consumption: 325.2 kg. The calculation formulas are as follows:

$$\frac{19,667.05\ \text{t}}{2.2\ \text{t/m}^3 \times 1000} \times \left(1\ \text{km} \times 1579.8\ \text{kg/km} + \frac{2\ \text{km}}{0.5} \times 142.22\ \text{kg/km}\right) = 19,208.27\ \text{kg} \tag{A9}$$

$$0.03\ \text{kg/yuan} \times 10 \times 216.8\ \text{yuan/d} \times 5\ \text{d} = 325.2\ \text{kg} \tag{A10}$$

(3) CO_2 emissions from the paving process:

The total asphalt production capacity of all four options is 240 t/h, so the CO_2 emissions from the paving process are the same. Referring to Appendix A and Table A11, the calculations are as follows.

The CO_2 emission from the paving process is 8581.36 kg, and the CO_2 emission from labor consumption is 65.04 kg. The calculation formulas are as follows:

$$\frac{19,667.05\ t}{2.2\ \text{t/m}^3 \times 1000} \times 959.93\ \text{kg} = 8581.36\ \text{kg} \tag{A11}$$

$$0.03\ \text{kg/yuan} \times 2 \times 216.8\ \text{yuan/d} \times 5\ \text{d} = 65.04\ \text{kg} \tag{A12}$$

(4) CO_2 emissions from the milling process:

The total asphalt production capacity of all four options is 240 t/h, so the CO_2 emissions from the milling process are the same. Referring to Appendix A and Table A12, the calculations are as follows.

The CO_2 emission from the milling process is 6670.75 kg, and the CO_2 emission from labor consumption is 162.6 kg. The calculation formulas are as follows, respectively:

$$\frac{19,667.05\ \text{t}}{2.2\ \text{t/m}^3 \times 1000} \times 678.368\ \text{kg} = 6064.32\ \text{kg} \tag{A13}$$

$$0.03\ \text{kg/yuan} \times 5 \times 216.8\ \text{yuan/d} \times 5\ \text{d} = 162.6\ \text{kg} \tag{A14}$$

(5) CO_2 emissions from ventilation processes:

Referring to Appendix A and Table A13, the calculations are as follows.

The CO_2 emission from the ventilation process is 4640 kg. The calculation formulas are as follows:

$$2 \times 58\ \text{kg/unit/h} \times 5 \times 8 = 4640\ \text{kg} \tag{A15}$$

References

1. Anderson, M. Climate Change 2014: Synthesis Report. *Libr. J.* **2016**, *141*, 28.
2. Renard, S.; Corbett, B.; Swei, O. Minimizing the global warming impact of pavement infrastructure through reinforcement learning. *Resour. Conserv. Recycl.* **2021**, *167*, 105240. [CrossRef]
3. Singh, A.; Vaddy, P.; Biligiri, K.P. Quantification of embodied energy and carbon footprint of pervious concrete pavements through a methodical lifecycle assessment framework. *Resour. Conserv. Recycl.* **2020**, *161*, 104953. [CrossRef]
4. Pranav, S.; Lahoti, M.; Shan, X.; Yang, E.; Muthukumar, G. Economic input-output LCA of precast corundum-blended ECC overlay pavement. *Resour. Conserv. Recycl.* **2022**, *184*, 106385. [CrossRef]
5. Liu, Q.; Cai, M.; Yu, B.; Qin, S.; Qin, X.; Zhang, J. Life cycle assessment of greenhouse gas emissions with uncertainty analysis: A case study of asphaltic pavement in China. *J. Clean. Prod.* **2023**, *411*, 137263. [CrossRef]
6. Zhu, S.; Qin, X.; Xu, Z.; Xing, M. Life cycle assessment of energy consumption and carbon emissions of a green maintenance material for asphalt pavement: Warm mix OUFC-5. *J. Clean. Prod.* **2023**, *428*, 139481. [CrossRef]
7. Suh, S.; Lenzen, M.; Treloar, G.J.; Hondo, H.; Horvath, A.; Huppes, G.; Jolliet, O.; Klann, U.; Krewitt, W.; Moriguchi, Y.; et al. System boundary selection in life-cycle inventories using hybrid approaches. *Environ. Sci. Technol.* **2004**, *38*, 657–664. [CrossRef]
8. Moreau, V.; Bage, G.; Marcotte, D.; Samson, R. Statistical estimation of missing data in life cycle inventory: An application to hydroelectric power plants. *J. Clean. Prod.* **2012**, *37*, 335–341. [CrossRef]
9. Wang, C.; Chang, Y.; Zhang, L.; Chen, Y.; Pang, M. Quantifying uncertainties in greenhouse gas accounting of biomass power generation in China: System boundary and parameters. *Energy* **2018**, *158*, 121–127. [CrossRef]
10. Bullard, C.W.; Penner, P.S.; Pilati, D.A. Net energy analysis: Handbook for combining process and input-output analysis. *Resour. Energy* **1978**, *3*, 267–313. [CrossRef]
11. Lave, L.B. Using input-output analysis to estimate economy-wide discharges. *Environ. Sci. Technol.* **1995**, *9*, 420A–426A. [CrossRef]
12. Wang, C.; Malik, A.; Wang, Y.; Chang, Y.; Lenzen, M.; Zhou, D.; Pang, M.; Huang, Q. The social, economic, and environmental implications of biomass ethanol production in China: A multi-regional input-output-based hybrid LCA model. *J. Clean. Prod.* **2020**, *249*, 119326. [CrossRef]
13. Heijungs, R.; Sun, S. The computational structure of life cycle assessment. *Int. J. Life Cycle Assess.* **2002**, *5*, 314. [CrossRef]
14. Malik, A.; Lenzen, M.; Geschke, A. Triple bottom line study of a lignocellulosic biofuel industry. *GCB Bioenergy* **2016**, *1*, 96–110. [CrossRef]
15. Wang, C.; Zhang, L.; Chang, Y.; Pang, M. Biomass direct-fired power generation system in China: An integrated energy, GHG emissions, and economic evaluation for Salix. *Energy Policy* **2015**, *84*, 155–165. [CrossRef]
16. Yang, J.; Zhang, L.; Wang, C.; Cai, Y.; Hao, Y. Energy consumption and greenhouse gas emission of an offshore windfarm in China: A hybrid life cycle assessment perspective. *Acta Sci. Circumstantiae* **2017**, *37*, 786–792.
17. Chen, Z.; Guo, Y.; Guo, C. Prediction of GHG emissions from Chengdu Metro in the construction stage based on WOA-DELM. *Tunn. Undergr. Space Technol.* **2023**, *139*, 105235. [CrossRef]
18. Zhao, J.; Kou, L.; Jiang, Z.; Lu, N.; Wang, B.; Li, Q. A novel evaluation model for carbon dioxide emission in the slurry shield tunnelling. *Tunn. Undergr. Space Technol.* **2022**, *130*, 104757. [CrossRef]
19. Jassim, H.S.H.; Lu, W.; Olofsson, T. Predicting energy consumption and CO_2 emissions of excavators in earthwork operations: An artificial neural network model. *Sustainability* **2017**, *9*, 1257. [CrossRef]
20. Chi, L.; Zhang, D.; Jia, M.; Ren, Z. Implementation of vector hysteresis model utilizing enhanced neural network based on collaborative algorithm. *IEEE Access* **2020**, *8*, 34162–34169. [CrossRef]

21. Lu, M.; Fang, S.; Li, G.; Wang, W.; Tan, X.; Wu, W. Optimization of adsorption performance of cerium-loaded intercalated bentonite by CCD-RSM and GA-BPNN and its application in simultaneous removal of phosphorus and ammonia nitrogen. *Chemosphere* **2023**, *336*, 139241. [CrossRef]
22. Kayalvili, S.; Selvam, M. Hybrid SFLA-GA algorithm for an optimal resource allocation in cloud. *Clust. Comput.* **2019**, *22*, S3165–S3173. [CrossRef]
23. Liu, Y.; Wang, Y.; An, D. Life-cycle CO_2 emissions and influential factors for asphalt highway construction and maintenance activities in China. *Int. J. Sustain. Transp.* **2018**, *12*, 497–509. [CrossRef]
24. Liu, N.; Wang, Y.; Bai, Q.; Liu, Y.; Wang, P.S.; Xue, S.; Yu, Q.; Li, Q. Road life-cycle carbon dioxide emissions and emission reduction technologies: A review. *J. Traffic Transp. Eng.* **2022**, *9*, 532–555. [CrossRef]
25. Liu, Q.; Yi, X.; Falchetto, A.C.; Wang, D.; Yu, B.; Qin, S. Carbon emissions quantification and different models comparison throughout the life cycle of asphalt pavements. *Constr. Build. Mater.* **2024**, *411*, 134323. [CrossRef]
26. Alam, M.R.; Hossain, K.; Bazan, C. Life cycle analysis for asphalt pavement in Canadian context: Modelling and application. *Int. J. Pavement Eng.* **2022**, *23*, 2606–2620. [CrossRef]
27. Santos, J.; Bressi, S.; Cerezo, V.; Lo Presti, D.; Dauvergne, M. Life cycle assessment of low temperature asphalt mixtures for road pavement surfaces: A comparative analysis. *Resour. Conserv. Recycl.* **2018**, *138*, 283–297. [CrossRef]
28. *JTG/T 3820—2018*; Guidelines for the Preparation of Investment Estimates for Highway Construction Projects. People's Communications Press: Beijing, China; Ministry of Transport: Beijing, China, 2018.
29. Huijbregts, M.; Gilijamse, W.; Ragas, A.; Reijnders, L. Evaluating uncertainty in environmental life-cycle assessment: A case study comparing two insulation options for a Dutch one-family dwelling. *Environ. Sci. Technol.* **2003**, *37*, 2600–2608. [CrossRef]
30. Santero, N.J.; Masanet, E.; Horvath, A. Life-cycle assessment of pavements. Part I: Critical review. *Resour. Conserv. Recycl.* **2011**, *55*, 801–809. [CrossRef]
31. AzariJafari, H.; Yahia, A.; Ben Amor, M. Life cycle assessment of pavements: Reviewing research challenges and opportunities. *J. Clean. Prod.* **2016**, *112*, 2187–2197. [CrossRef]
32. Liao, X.; Tian, Y.; Gan, Y.; Ji, J. Quantifying urban wastewater treatment sector's greenhouse gas emissions using a hybrid life cycle analysis method—An application on Shenzhen city in China. *Sci. Total Environ.* **2020**, *745*, 141176. [CrossRef]
33. Wang, Z.; Wang, Q.; Wang, C.; Yang, Z. A comparative study of China's green aircraft carbon emissions based on hybrid life cycle assessment. *J. Propuls. Technol.* **2024**, *45*, 26–36.
34. Holland, J.H. *Adaptation in Natural and Artificial Systems*; University of Michigan Press: Ann Arbor, MI, USA, 1975.
35. Tian, Y. Using a back propagation network based on genetic algorithm to study influence factors of carbon dioxide emissions in China. *Sci. Technol. Ind.* **2018**, *18*, 68–76.
36. Zhang, H. Simulation-Based Estimation of Fuel Consumption and Emissions of Asphalt Paving Operations. *J. Comput. Civ. Eng.* **2015**, *29*, 2. [CrossRef]
37. Liu, Y.; Liu, H.; Wu, M.; Wang, Y. Calculation of energy consumption and influencing factors of asphalt pavement construction. *Road Mach. Constr. Mech.* **2016**, *33*, 108–112.
38. Li, C. Carbon Emission Calculation of Asphalt Surface of Highway during the Construction Period. Master's Thesis, Changsha University of Science & Technology, Changsha, China, 2018.
39. Wan, J. The Study on Optimization of Carbon Emission from Expressway Pavement Construction Based on LCA-Taking H-G Expressway as An Example. Master's Thesis, Hefei University, Hefei, China, 2022.
40. Huang, Y.; Qiao, Z.; Zhang, H. Evaluation of an economy-technology-green development system for asphalt pavement construction in China based on synergetics. *J. Clean. Prod.* **2021**, *289*, 125132. [CrossRef]
41. Wang, F.; Hoff, I.; Yang, F.; Wu, S.; Xie, J.; Li, N.; Zhang, L. Comparative assessments for environmental impacts from three advanced asphalt pavement construction cases. *J. Clean. Prod.* **2021**, *297*, 126659. [CrossRef]
42. Zhang, H.; Lepech, M.D.; Keoleian, G.A.; Qian, S.; Li, V.C. Dynamic life-cycle modeling of pavement overlay systems: Capturing the impacts of users, construction, and roadway deterioration. *J. Infrastruct. Syst.* **2010**, *16*, 299–309. [CrossRef]
43. Liu, B.; Wang, S.; Liang, X.; Han, Z. Carbon emission reduction prediction of new energy vehicles in China based on GRA-BiLSTM model. *Atmos. Pollut. Res.* **2023**, *14*, 1018659. [CrossRef]
44. Jiang, H.; Yin, J.; Wei, D.; Luo, X.; Ding, Y.; Xia, R. Industrial carbon emission efficiency prediction and carbon emission reduction strategies based on multi-objective particle swarm optimization-backpropagation: A perspective from regional clustering. *Sci. Total Environ.* **2024**, *906*, 167692. [CrossRef]
45. Wang, H. Study on Carbon Emission Calculation and Prediction of Guangxi Expressway Construction Period. Master's Thesis, Guangxi University, Nanning, China, 2022.
46. Zhang, Q.; Xu, J.; Zhang, J. Applied research on life cycle assessment (LCA) methodology for pavement engineering. *J. China Foreign Highw.* **2015**, *35*, 346–350.
47. *DB 34/T 3679-2020*; Specification for Construction of Asphalt Mixtures Mixing Plant. Anhui Provincial Market Supervision Administration: Hefei, China, 2020.

48. *GB/T 17808-2021*; Road Construction and Maintenance Machinery and Equipment-Asphalt Mixing Plant. State Administration for Market Regulation: Beijing, China, 2021.
49. Cui, P. The Establishment of a Life-Cycle Carbon Emission Factor Database for Buildings and Related Research. Master's Thesis, Southeast University, Nanjing, China, 2015.
50. *GB/T 2589-2020*; General Rules for the Calculation of Comprehensive Energy Consumption. State Administration for Market Regulation, Standardization Administration of China: Beijing, China, 2020.
51. *JTGT 3833—2018*; Cost Quota for Highway Engineering Machinery Team. Ministry of Transport of the People's Republic of China: Beijing, China, 2018.